Roughness and growth in a continuous fluid invasion model

Inbal Hecht and Haim Taitelbaum

Department of Physics, Bar-Ilan University, Ramat-Gan 52900, Israel

(Received 10 September 2003; revised manuscript received 29 March 2004; published 21 October 2004)

We have studied interface characteristics in a continuous fluid invasion model, first introduced by Cieplak and Robbins [Phys. Rev. Lett. **60**, 2042 (1988)]. In this model, the interface grows as a response to an applied quasistatic pressure, which induces various types of instabilities. We suggest a variant of the model, which differs from the original model by the order of instabilities treatment. This order represents the relative importance of the physical mechanisms involved in the system. This variant predicts the existence of a third, intermediate regime, in the behavior of the roughness exponent as a function of the wetting properties of the system. The gradual increase of the roughness exponent in this third regime can explain the scattered experimental data for the roughness exponent in the literature. The growth exponent in this model was found to be around zero, due to the initial rough interface.

I. INTRODUCTION

Fluid flow in porous media is an important process in nature, with applications in a wide variety of technological areas, such as wetting and drying processes, painting, and hydrology. In the past two decades, many papers have addressed this issue, both experimentally and theoretically [1–22]. Most experiments were done using a Hele-Shaw cell [8–11,13,17], tubes network [5–7], or paper [12], with fluids such as water, glycerol, or ink. Several models were introduced in order to describe flow dynamics and interface characteristics under nonequilibrium conditions. In the invasion percolation (IP) model [23–25], fluid invasion is mapped onto the problem of percolation on a network of pores and throats. In standard percolation, and thus in various IP models, the approach to the percolation transition is universal, and depends neither on the geometry of the network nor on the wetting properties of the invading fluid. However, experimental studies show a significant difference in the patterns and dynamics of wetting (W) and nonwetting (NW) fluid invasion [6,7]. Cieplak and Robbins (CR) [1–4], led by experimental evidence [5–8], have constructed an innovative fluid invasion model, which includes the microscopic geometry of the porous medium and the wetting properties of the invading fluid. The model is based on the growth of the interface as a response to an applied pressure in a quasistatic process. Three basic types of instabilities then occur, and each unstable section of the interface moves to the next stable or nearly stable configuration. The main feature of the CR model is the transition from a compact, self-affine interface (depinning) when the fluid is more wetting, to a fractal structure (percolation) in the NW case. This model was mainly studied in its percolation regime, in particular with respect to finger width and fractal dimension. General scaling laws were obtained, both for the percolation and the depinning regimes, but only with respect to the invaded volume and external surface.

The CR model has been found to agree quite well with some of the experimental results. However, other experimental results for very similar systems but with different fluids indicate that the interface dynamics depends on the specific wetting properties of the system. In the current work, motivated by recent experimental systems of interface dynamics [26,27], we are interested in studying the detailed growth dynamics of the CR model. In particular, we focus on the roughness and growth exponents, α and β, respectively, and their possible dependence on the wetting properties of the fluid. We shall do so by first examining in detail the relative importance and order of instabilities occurrence and removal in the CR model. As a result of this examination, we suggest a variant of the model, which is more consistent with respect to the instabilities statistics. This variant explains some scatter in the available experimental data for the roughness exponent, which is not explained by the current model results.

The paper is organized as follows. In Sec. II, we describe the fluid invasion model. In Sec. III, we present our results for instability statistics in both variants of the model. Section IV is devoted to calculation of interface characteristics in both models, as a function of the wetting properties of the fluid. From this calculation we infer the existence of an intermediate, new regime, of the behavior of the roughness exponent, and discuss these results with respect to experimental data. In Sec. V, we summarize the results.

II. THE FLUID INVASION MODEL

In this section, we describe the fluid invasion model, first introduced by CR [1,2]. The model system (Fig. 1) is a two-dimensional array of disks, placed on a triangular lattice, with L grid points per row and per column. The interface consists of a sequence of arcs between pairs of disks. The angle θ between the arc and the disk is determined by the wetting properties of the fluid. $\theta=0°$ corresponds to the W limit, and $\theta=180°$ corresponds to the NW limit. Each arc has the radius $r=\gamma/P$, where γ is the surface tension and P is the pressure difference, which is uniform in the entire system.

There are three types of instabilities (Fig. 2) related to the different growth mechanisms of the system [1–3].

(i) "Burst." When the pressure is above a critical value, there does not exist an arc connecting the disks in the given θ (temporarily, the interface is represented by the arc with the smaller radius possible).
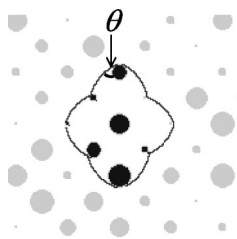
FIG. 1. Initial configuration of arcs. In this figure, $\theta = 25°$ and the magnification is $\times 12$.

(ii) "Touch." The arc connecting two disks intersects another disk or extends beyond a disk that has not yet been connected.

(iii) "Overlap." Two adjacent arcs intersect.

The initial interface has a shape of a ring around the center of the system, and is stable at an applied pressure P. The dynamics is a stepwise process where each unstable section of the interface moves to the next stable or nearly stable configuration. The pressure is slightly increased, and all arcs are recalculated according to the new radius. Every unstable arc is replaced by a stable one, according to the type of instability. The different types of instabilities represent different physical phenomena, resulting in different microscopic growth mechanisms.

Burst instabilities are related to pressure; they are eliminated by advancing the interface to the nearest disk that lies in the angle subtended by the arc [Fig. 2(a)]. Occurrence of burst instabilities is independent of the lattice structure and depends only on the wetting angle θ, the pore size (i.e., the distance between the disks), and the arc radius, which is determined by the pressure. Touch is a local mechanism, like burst, but its occurrence depends on the size of the forward disk and on the direction of flow. Touch instabilities are eliminated by replacing the unstable arc with two new arcs, connecting the "touched" disk with each of the original disks [Fig. 2(b)]. The advancement of the interface depends on the lattice structure and on the driving force (pressure), which is similar to depinning. The removal of overlaps is done by replacing the two overlapping arcs with a single new arc [Fig. 2(c)]. The disk that is common to the intersecting arcs is removed from the interface. This mechanism imitates the effect of surface tension and wetting.

When a totally stable configuration is achieved, the pressure P is increased again, until growth resumes. The pressure increment is very small (10^{-3}–10^{-4} of the critical pressure), so the process may be considered quasistatic. As a result of each pressure increment, only one or two new instabilities
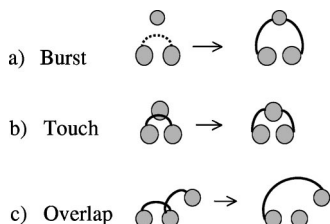
FIG. 2. Instabilities and their removal. (a) Burst; (b) Touch; (c) Overlap.
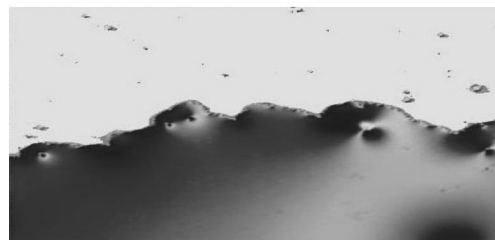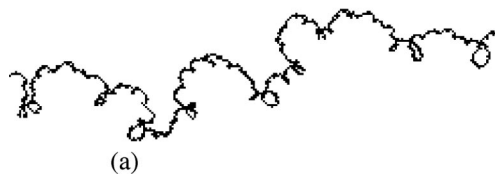
FIG. 3. (a) Typical interface in the TBO model, for $\theta = 25°$ after $O(10^3)$ steps; (b) experimental system of mercury spread on thin silver film [26,27].

may occur. Near the critical pressure, removing these instabilities will cause new ones to appear. At the critical pressure, this chain process continues and the droplet grows infinitely without any further pressure increase. The constant but slow increase of the pressure is analogous to constant flow rate in experimental systems [5,7,21].

The results of this model indicated a dynamical critical transition at a critical angle θ_c [1–3] above which the growth patterns are fractal (NW limit) and below which they correspond to depinning (W limit). It was argued [1,2,16] that since touches and particularly bursts are *local* mechanisms, which can be included in percolation models, they play the dominant role in the percolative, nonwetting limit (above θ_c). In contrast, since an overlap depends on the configuration of adjacent arcs, it is a *global* instability, which becomes more likely as θ decreases, in particular below θ_c. Its effect is to smooth the interface and to induce a cooperative motion in this wetting/depinning limit. As CR point out [1], the variation in importance of the growth mechanisms with θ leads to dramatic changes in the pattern of the growing interface. Thus, since our primary goal is to study interface characteristics, we must give special attention to the order of instabilities removal.

In principle, the order of instability removal is arbitrary. Cieplak and Robbins discuss this issue [2] and explain why the touches should be eliminated first, then overlaps, and finally bursts (TOB). They have used this order of instability removal in all of their simulations. However, in light of the different role played by each type of instability in each regime, the justification for this order should be examined in greater detail. In the following, we will show that eliminating the bursts before the overlaps (TBO order) produces interfaces that resemble experimental results, both qualitatively (Fig. 3) and quantitatively (roughness exponent values). The TBO order is relevant to systems in which surface tension plays a secondary role with respect to other physical mechanisms. Moreover, we will show the self-consistency of this removal order with respect to instability statistics.
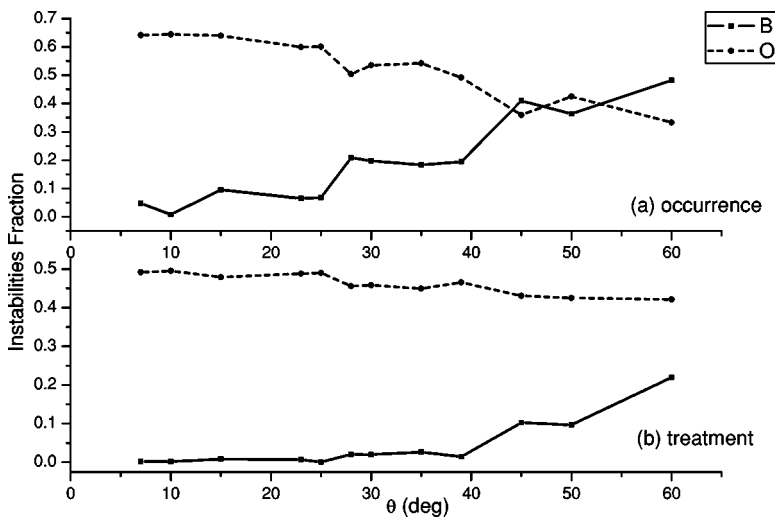
FIG. 4. Instabilities analysis in the TOB model. The fraction of (a) occurrence and (b) treatment for burst (solid line) and overlap (dashed line) instabilities, as a function of θ.

III. INSTABILITY STATISTICS

We performed numerical calculations of the model using systems of sizes $L=1200$ and $L=2500$ grid points. The disks were placed alternately on even or odd columns (i.e., 600 or 1250 disks per row/column), creating effectively a triangular lattice. The disk sizes were equally distributed in the range [0.05,0.49] lattice units. In order to follow the instabilities occurrence and treatment rate, we have designated six different counters for the three types of instability. During the growth process, whenever an instability occurs, a counter is updated. Whenever an instability is treated, another counter is updated. There is an important difference between existing and treated instabilities according to the order of treatment. For example, the number of touch instabilities out of the total number of instabilities may be low, but since they are the first to be treated, the number of the treated touches out of the total number of treated instabilities is much higher. The counters values were divided by the sum of all three relevant counters and these ratios were averaged during the growth process. The characteristic ratios of each system were also averaged over several runs (four to eight for each value of θ). We performed this statistics for both the TOB and TBO versions of instabilities treatment order.

In Figs. 4(a) and 4(b), we show the fraction of each type of the existing and treated burst and overlap instabilities as a function of the wetting angle, in the TOB model. It can be seen that when $\theta \sim 28°$, there is an increase in the occurrence of burst instabilities and a decrease in the amount of overlaps. However, this increase is not given a proper treatment, as the number of *treated* burst instabilities does not change and remains close to zero. It is only around $\theta \sim 50°$ where an increase in the number of treated bursts starts to show up. Therefore, it seems that the region between $\theta \sim 28°$ (which will be referred to later as θ^*) and $\theta \sim 50°$ (which is actually θ_c) is "missed" by the TOB treatment order.

In Figs. 5(a) and 5(b), we show the corresponding plots for the TBO version. Here also the occurrence of burst instabilities starts to increase around the same angle $\theta^* \sim 28°$. However, one can clearly see that in this case the number of treated bursts does increase gradually starting at this angle. This means that the TBO order is more self-consistent than the TOB in the sense that the treatment rate of the burst instabilities does properly follow their occurrence rate.

In Fig. 6, we compare the amount of treated burst instabilities in the TOB and TBO cases, as a function of the angle θ. It is easy to notice the gradual growth starting at $\theta^* \sim 28°$ in the TBO case, which is very different from the
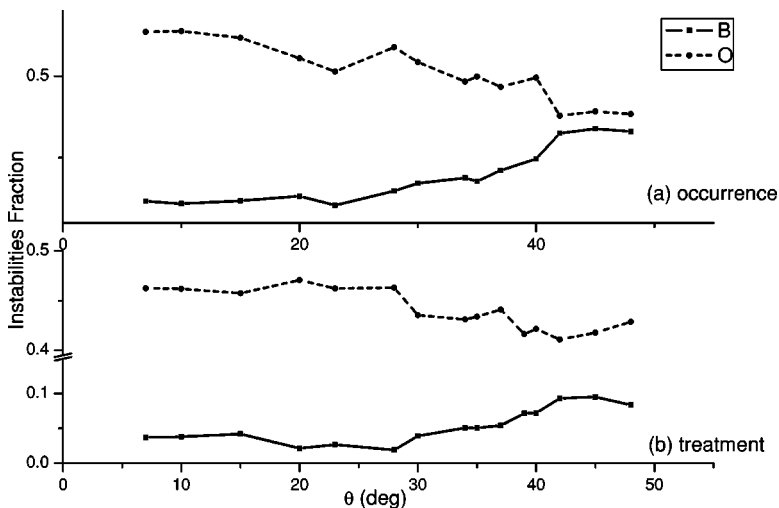
FIG. 5. Instabilities analysis in the TBO model. The fraction of (a) occurrence and (b) treatment for burst (solid line) and overlap (dashed line) instabilities, as a function of θ.
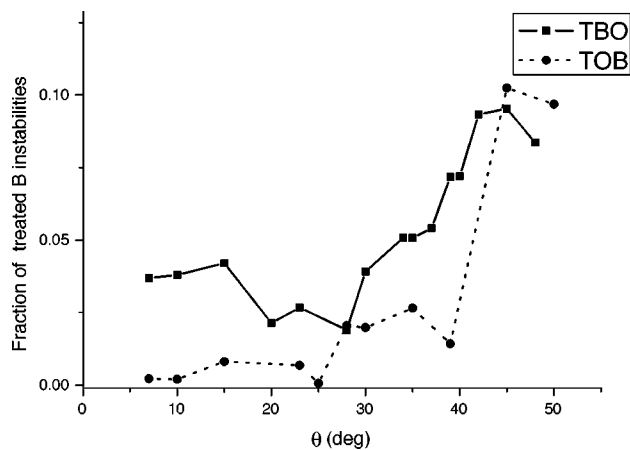
FIG. 6. Fraction of treated burst instabilities in the TBO (solid line) and TOB (dashed line) models, as a function of θ.

sharp increase in the TOB case, occurring around $\theta_c \sim 50°$, following a region $\theta^* < \theta < \theta_c$ in which the treatment does not follow the occurrence increase.

As was pointed out by CR [1,2], and can be also inferred from Figs. 4 and 5, the dominant instability *above* θ_c is burst. This may give priority to TBO in this region. However, when there is a total dominance of one of the instabilities, the treatment order is arbitrary, as is the case in the region $\theta < \theta^*$. It is only when the number of two types of instabilities becomes comparable (as we have shown to be the case in the region $\theta^* < \theta < \theta_c$) that the treatment order is important. Therefore, it seems that the TOB version is adequate for $\theta > \theta_c$. In any case, since our main aim is to study the interface characteristics in the wetting regime ($\theta < \theta_c$), we leave the detailed study of the percolative region for future work.

IV. ROUGHNESS AND GROWTH EXPONENTS

The width w of the interface is defined as [23,25]

$$w^2 \sim \langle h^2(x,t) \rangle - \langle h(x,t) \rangle^2, \tag{1}$$

where $h(x,t)$ is the interface height in point x at time t. This width w is related to the time t and length L by two scaling exponents α and β, according to

$$w \sim \begin{cases} t^\beta, & t \ll t_0 \\ L^\alpha, & t \gg t_0, \end{cases} \tag{2}$$

where $t_0 \sim L^{\alpha/\beta}$, α is the roughness exponent and β is the growth exponent.

A. Roughness exponent

The value of α, the roughness exponent, which describes the correlations along the interface, usually reflects the nature of the growth mechanism in the system. Martys, Cieplak, and Robbins [3] calculated this exponent for the wetting regime (below θ_c) and found $\alpha = 0.81 \pm 0.05$ for $\theta = 25°$ as a representative angle for this regime. It was claimed that this value of α agrees very well with experimental data on wetting invasion [8–11], unlike most growth

models (e.g., Kardar-Parisi-Zhang (KPZ) [29]) which give $\alpha = 0.5$. In fact, as was pointed out by Roux and Hansen [16], as well as later by Albert *et al.* [18], there exists some scatter in the determination of α from experimental results, most of them performed in Hele-Shaw cells. The reported values of roughness exponents in the literature are 0.73 [8], 0.91 [9], 0.81 [11], 0.63 [12], and 0.77 [17]. This scatter was the subject of a published controversy in the literature [8–10] without a definitive conclusion. These data pose the question on how general is the $\alpha = 0.81$ result obtained for $\theta = 25°$ in the CR model. Specifically, one may ask if this result is valid for the entire wetting regime below θ_c.

Thus, our aim is to explore the possible influence of θ, which represents the wetting properties of the invading fluid, on the roughness exponent of the growing interface. In the previous section, we have shown that the wetting region is sensitive to the order of instabilities removal. Hence, we analyzed the roughness exponent for both TBO and TOB models. The analysis was done on the advancing interface and not on the infinite final cluster, in order to imitate the experimental systems [26,27]. As will be shown later, the initial interface is rough enough so that α can be calculated from relatively early stages of the growth process.

Practically speaking, the task of determining the exact shape of the interface line depends on the resolution of the graphical drawing of that interface. Hence two magnification scales were used in the graphical demonstration, to ensure the generality of the roughness exponent's behavior and its independence of length scale. Half of the systems were drawn with one pixel per point, and the other half with two pixels per point. In principle, the higher the magnification is, the smaller the details that can be observed, but in fact no significant difference in the calculated values was observed. The interface was graphically analyzed at different times in the range 2000–10 000 time steps, where a single time step is defined as one iteration on the entire interface.

In order to analyze interface characteristics, and to avoid the artificial correlations of the circular shape, the interface was cut to nonoverlapping, straight-line segments. The typical segment size, L_0, that could be considered straight, depends strongly on the interface roughness. Interfaces with small roughness exponent α (α closer to 0.6) tended to grow circularly; in such cases, the entire circular interface length was ~ 3000 pixels (which are equivalent to 3000 or 1500 lattice grid points, depending on the magnification used), and the typical segment length L_0 was ~ 300 pixels. For interfaces with larger α, the growth was less circular and longer segments, up to ~ 600 pixels, could be taken. For each value of θ in the range 7–50 degrees, we created two to four lattices with random disk configurations and four to six segments were taken from each system. For every straight segment of length L_0, we took all the possible subsegments with length L, for every L in the range $[0, L_0/2]$. The width of the interface in every subsegment was calculated by the mean-square-root deviation from the average interface position, and then averaged over all subsegments with the same L. A graph of $\log(w)$ versus $\log(L)$ was plotted, thus the slope of the graph gives the roughness exponent for the specific segment. Typical graphs are represented in Figs. 7(a) and 7(b), each for a different value of the angle θ, $\theta = 25°$ in Fig. 7(a)
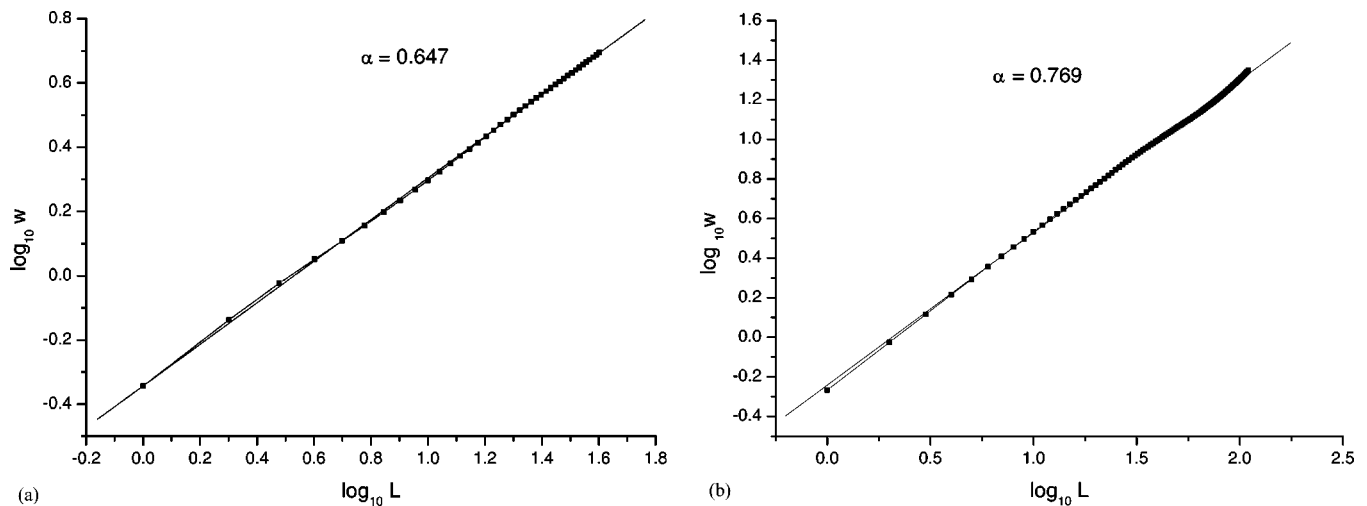
FIG. 7. Typical interface analysis for the TBO model. (a) $\theta=25°$; (b) $\theta=37°$.

and $\theta=37°$ in Fig. 7(b). Both plots, which give different roughness exponents ($\alpha=0.647$ for $\theta=25°$ and $\alpha=0.769$ for $\theta=37°$), were produced using the TBO variant of the model.

1. TOB (touch, overlap, burst)

In this version, the overlap instabilities were eliminated before the burst instabilities, as was done in the original CR model [1–3]. The results for the roughness exponent in the TOB model are summarized in Fig. 8(a). Each point in the graph is the average slope of $w(t)$, as in Fig. 7. We found that there are two regimes, separated by the critical angle θ_c, as predicted by CR [1–3]. Below $\theta_c \sim 50°$, the structure is compact; above θ_c, the structure is fractal. This transition from a compact, self-affine to a fractal structure was verified by measuring the fractal dimension of the interface line. Below $\theta_c \sim 50°$, the system is basically one-dimensional (1.00 ± 0.03), whereas above θ_c we obtain a fractal dimension of 1.15 ± 0.05.

In the compact region below θ_c, we obtain for the roughness exponent the result of $\alpha \sim 0.7$. This value is lower than the CR result of $\alpha \sim 0.81$. We believe that this is due to different graphical accuracy, since the value of the roughness exponent α is sensitive to artificial smoothing. Reducing the graphical accuracy, for example by drawing only centers of arcs, causes an effective smoothing of the interface, and therefore increases the value of α. In our system, we took care of fully detailed drawing of all arcs, so the circular nature of the interface units influenced the results for α. We believe that this is the reason for the differences between our results and the CR results. Indeed, for a graphically smoothed interface, we have reproduced the CR result of $\alpha=0.81 \pm 0.05$ for $\theta=25°$.

2. TBO (touch, burst, overlap)

The results for the TBO model are summarized in Fig. 8(b). Within the compact regime below θ_c we find two sub-regimes. For small wetting angles ($\theta < \theta^*, \theta^*=28°$), the
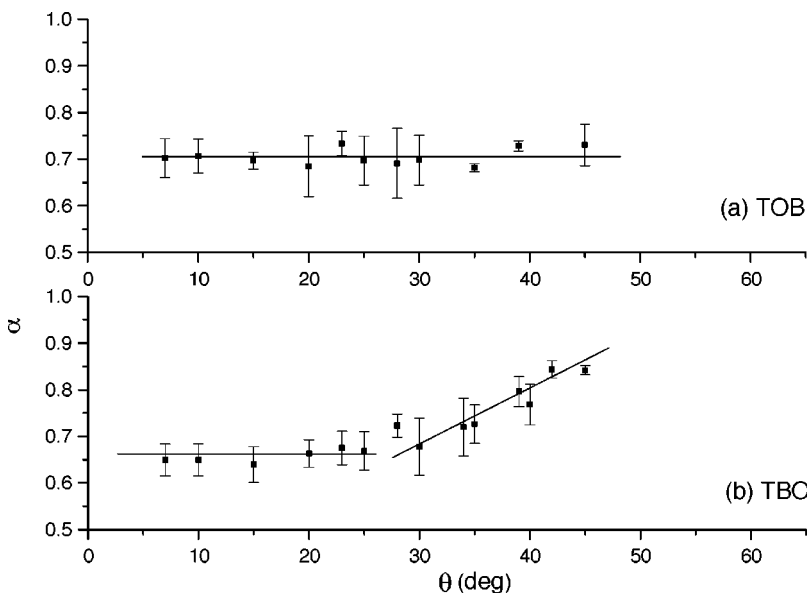
FIG. 8. Roughness exponent α vs wetting angle θ below θ_c: (a) in the TOB model; (b) in the TBO model. The solid lines show the approximately constant value of α in the TOB model (a), and the two-region behavior of α in the TBO model (b), a constant below $\theta^*=28°$, and a linear growth above it.
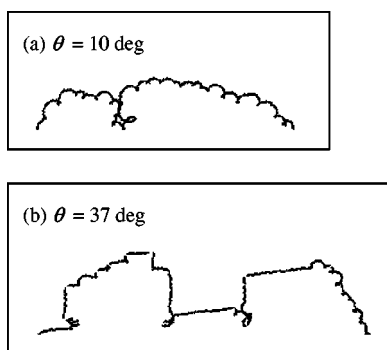
FIG. 9. Typical interfaces in the TBO model. (a) $\theta=10°$; (b) $\theta=37°$.

roughness exponent α is around 0.65, while for larger values of θ ($\theta^* < \theta < \theta_c$) we found that α grows monotonically, approximately linearly with θ. This is very different from the TOB case, since the transition to the fractal regime is gradual and not sharp, and the value of α is *not* constant. Regarding the system dimensionality, preliminary results give a dimension of 1.02 ± 0.01 below θ_c and 1.165 ± 0.015 above it. Detailed analysis of the fractal dimension, in particular above θ_c, in both TBO and TOB, will be discussed elsewhere.

The dependence of α on θ in the wetting regime shows that the exact dynamics of the interface depends on the specific wetting properties of the fluid. The prediction of this third regime of weak wetting in the TBO version is consistent with our earlier discussion of instabilities. We believe that the TBO must be the proper instability removal order in this regime.

Typical interfaces below and above $\theta^* \sim 28°$ are represented in Fig. 9. It is easy to notice that although the interface of $\theta=37°$ [Fig. 9(b)] is compact, its geometrical structure (self-affinity) looks very different from the interface of $\theta=10°$ [Fig. 9(a)].

3. TOB versus TBO

The results for the roughness exponent presented in the previous two subsections indicate that there are two basic differences between the TBO and the TOB results. The first is a different value for the *constant* roughness exponent for $\theta < \theta^*$, and the second is a totally different behavior in a new region, $\theta^* < \theta < \theta_c$.

The different constant value of α is a direct consequence of the treatment order. An interface may have a large roughness exponent in one of the two opposite circumstances, namely when the interface is very smooth or when the interface is very rough but self-similar. In our model, a smooth interface will be obtained if the main instability is overlap, while a self-similar interface will be obtained if the main instability is burst. In both cases, the roughness exponent will be large, namely close to 1. In the TBO version, the interfaces for small θ ($\theta < \theta^*$) have more overlaps but there are also bursts, thus the roughness exponent is about 0.65. This value is smaller than the corresponding TOB value (0.7), because there are more bursts and fewer overlaps than in the TOB case (as can be seen from Fig. 6). Generally

speaking, after an overlap is eliminated, the distance between the two edges of the created new arc is larger than the distances of the two original arcs. As a result, this new arc has a larger probability for burst and overlap instabilities to occur. If we remove overlaps before bursts (TOB), then all sizes of arcs will appear in the interface, including very large arcs, between very distant disks. But if we eliminate bursts first (TBO), then there will be a typical arc size, which is in the order of two to three lattice constants, and there will be no large arcs in the interface. Large arcs result in large α, and this is the reason why we obtain $\alpha=0.7$ in the TOB case and $\alpha=0.65$ in the TBO case.

The TOB results of the original CR model were used to explain the relatively high values of roughness exponent α (0.75–0.9) found in some experiments, as well as the difference between wetting and nonwetting fluids. However, the full spectrum of very different values of α for different fluids and experimental conditions *cannot* be explained by the constant value of α predicted by CR. For example, Horvath *et al.* used two different fluids in a Hele-Shaw cell, and obtained the values of 0.88 for water [9] and 0.81 for glycerol [11]. The different value of α for two different fluids can be explained only if the TBO version is used. Another example is due to He, Kahanda, and Wong [13], in their series of experiments in a Hele-Shaw cell. The roughness exponent α was measured in different cases, with several values of the capillary number. They found that the roughness exponent value is not constant but decreases when the capillary number increases. This dependence is also compatible only with the TBO results.

Our main result for the behavior of the roughness exponent, as a function of system parameters, in the TBO version, is the *three-regime behavior*, which resembles a similar finding by Tanguy, Gounelle, and Roux [19]. They have theoretically investigated the effect of the range of elastic interactions in the dynamical behavior of an elastic chain. The roughness exponent of the chain was measured for several values of the interaction decay exponent. They found three regimes. (i) A mean-field regime for slow decay interactions, where the roughness exponent is roughly constant. The interaction is evenly distributed over the system and the chain advances coherently, with a small value of the roughness exponent. (ii) A Laplacian regime for fast decay interactions, where the roughness exponent is also constant but has a higher value. (iii) An intermediate regime, in which the roughness exponent grows monotonically as a function of the decay exponent. As the interaction is more concentrated on nearest neighbors, different segments of the chain advance independently, and a higher value of roughness exponent is obtained. A clear crossover is noticed between these three regimes. This is very much like our system: for almost-complete wetting (small θ), the amount of overlaps is very high and the "interaction" between arcs is long-ranged. Therefore, the roughness exponent is small and constant. When the fluid is less wetting (namely larger θ), the local mechanism (burst) has a stronger effect and the roughness exponent increases monotonically. Above the critical angle θ_c, the roughness exponent is also constant and equal to 1 since the interface is fractal. This three-regime behavior can be obtained only with the TBO variant of the CR model.

In addition, the TBO version, where burst instabilities are eliminated before the overlaps, may be more appropriate for describing systems in which wetting and surface tension have a weaker influence than pressure effects. In the TOB model, the surface tension (overlaps) has more influence on the growth process than the local pressure (bursts). Therefore, we believe that the TOB model cannot describe experimental systems with chemical reactions. For example, in the experimental system of Be'er *et al.* [26,27], a mercury droplet spreads over a thin silver film, while chemically reacting with the film. In this system, the local chemical reaction mechanism is as strong as the global surface tension mechanism. The roughness exponent of the reaction front was found to be 0.66 [26], which is much lower than the TOB results. This value, which is much closer to the TBO results ($\alpha \sim 0.65$), supports this argument for such systems.

It is interesting to note that Hentschel and Family [30] suggested a dimensional analysis method for finding the scaling exponents and universality classes for different cases of the KPZ equation [29]. In the case of quenched disorder (when the noise is time-independent, also called the "QKPZ equation"), for rough surface and negligible surface tension one can obtain $\alpha = 4/(d+4)$, which yields $\alpha = 2/3$ in $d=2$. This is in very good agreement with the system of TBO order, in which surface tension forces are of least importance since overlap instabilities are the last to be treated.

B. Growth exponent

The growth exponent β was calculated by averaging the interface width for different length scales (as described above for the roughness exponent), in successive time steps. A single "time step" was defined as a single iteration on the entire interface. For the time interval in which β was calculated, this "time step" can be considered constant, since the radius is growing very slowly and the invaded volume is roughly the same. The results for a typical interface are shown in Fig. 10. The growth exponent β is found to be around zero. This result has been obtained in all cases, in both the TOB and the TBO models. This model result cannot be directly compared to experimental systems, since in this model any small initial interface is rather rough, being constructed of several distinct arcs. Any further growth causes the interface to advance, but does not increase its width significantly. In typical experimental systems, however, the interface is initially rather smooth, and becomes rougher as it
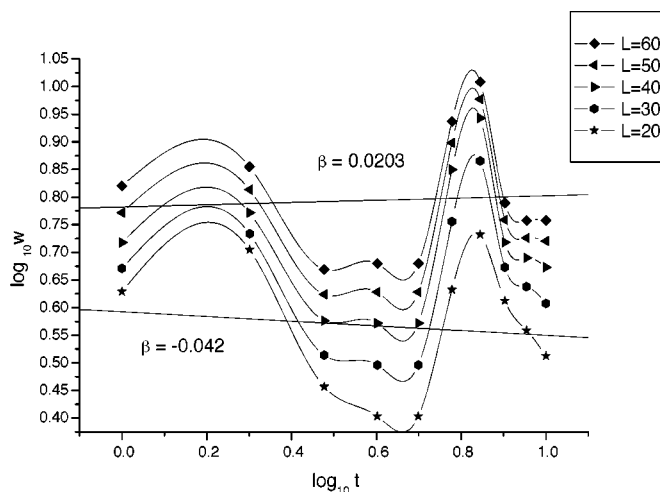
FIG. 10. Typical growth exponent analysis in the TBO model for $\theta = 25°$, at $L = 20$, 30, 40, 50, and 60 pixels and linear fits for $L = 20$ and $L = 60$.

grows. This means that the model cannot properly describe early time-dependent behavior. The nonmonotonic behavior of the function $w(t)$ shown in Fig. 10 is discussed in a more general context elsewhere [28].

V. SUMMARY

We have shown that the order of instability removal, in a fluid invasion model first introduced by Cieplak and Robbins, has a considerable impact on the interface roughness properties. This order is related to the physical properties of the system and to the mechanism that governs the growth. We have suggested and discussed an alternative removal order which seems to be more self-consistent. This model variant yields a different behavior for the roughness exponent in the system. In particular, it predicts a new regime, where the roughness exponent gradually changes with the wetting properties of the system. This finding explains the wide range of experimental results of α reported in the literature.

ACKNOWLEDGMENTS

[1] M. Cieplak and M. O. Robbins, Phys. Rev. Lett. **60**, 2042 (1988).

[2] M. Cieplak, and M. O. Robbins, Phys. Rev. B **41**, 11508 (1990).

[3] N. Martys, M. Cieplak, and M. O. Robbins, Phys. Rev. Lett. **66**, 1058 (1991).

[4] N. Martys, M. O. Robbins, and M. Cieplak, Phys. Rev. B **44**, 12294 (1991).

[5] R. Lenormand, and C. Zarcone, Phys. Rev. Lett. **54**, 2226

(1985).

[6] J. P. Stokes, D. A. Weitz, J. P. Gollub, A. Dougherty, M. O. Robbins, P. M. Chaikin, and H. M. Lindsay, Phys. Rev. Lett. **57**, 1718 (1986).

[7] R. Lenormand, E. Touboul, and C. Zarcone, J. Fluid Mech. **189**, 165 (1988).

[8] M. A. Rubio, C. A. Edwards, A. Dougherty, and J. P. Gollub, Phys. Rev. Lett. **63**, 1685 (1989).

[9] K. V. Horvath, F. Family, and T. Vicsek, Phys. Rev. Lett. **65**,

1388 (1990).

[10] M. A. Rubio, C. A. Edwards, A. Dougherty, and J. P. Gollub, Phys. Rev. Lett. **65**, 1389 (1990).

[11] K. V. Horvath, F. Family, and T. Vicsek, J. Phys. A **24**, L25 (1991).

[12] S. V. Buldyrev, A. L. Barabasi, F. Caserta, S. Havlin, H. E. Stanley, and T. Vicsek, Phys. Rev. A **45**, R8313 (1992).

[13] S. He, G. L. M. K. S. Kahanda, and P.-Z. Wong, Phys. Rev. Lett. **69**, 3731 (1992).

[14] C. S. Nolle, B. Koiller, N. Martys, and M. O. Robbins, Phys. Rev. Lett. **71**, 2074 (1993).

[15] C. S. Nolle, B. Koiller, N. Martys, and M. O. Robbins, Physica A **205**, 342 (1994).

[16] S. Roux and A. Hansen, J. Phys. I **4**, 515 (1994).

[17] A. Paterson, M. Fermigier, P. Jeniffer, and L. Limat, Phys. Rev. E **51**, 1291 (1995); A. Paterson, Ann. Phys. (Paris) **21**, 337 (1996).

[18] R. Albert, A. L. Barabasi, N. Carle, and A. Dougherty, Phys. Rev. Lett. **81**, 2926 (1998).

[19] A. Tanguy, M. Gounelle, and S. Roux, Phys. Rev. E **58**, 1577 (1998).

[20] M. Dubé, M. Rost, and M. Alava, Eur. Phys. J. B **15**, 691 (2000).

[21] A. Hernández-Machado, J. Soriano, A. M. Lacasta, M. A. Rodríguez, L. Ramírez-Piscina, and J. Ortín, Europhys. Lett. **55**, 194 (2001).

[22] H. J. Kim and I. Kim, J. Korean Phys. Soc. **40**, 1005 (2002).

[23] A. Bunde and S. Havlin, *Fractals and Disordered Systems* (Springer-Verlag, Berlin, 1991).

[24] D. Stauffer and A. Aharony, *Introduction to Percolation Theory* (Taylor & Francis, London, 1991).

[25] P. Meakin, *Fractals, Scaling and Growth Far From Equilibrium* (Cambridge University Press, Cambridge, 1998).

[26] A. Be'er, Y. Lereah, and H. Taitelbaum, Physica A **285**, 156 (2000).

[27] A. Be'er, Y. Lereah, I. Hecht, and H. Taitelbaum, Physica A **302**, 297 (2001).

[28] A. Be'er, I. Hecht, and H. Taitelbaum (unpublished).

[29] M. Kardar, G. Parisi, and Y. C. Zhang, Phys. Rev. Lett. **56**, 889 (1986).

[30] H. G. E. Hentschel and F. Family, Phys. Rev. Lett. **66**, 1982 (1991).